ISSN 1027-4510, Journal of Surface Investigation: X-ray, Synchrotron and Neutron Techniques, 2022, Vol. 16, No. 6, pp. 1041–1047. © Pleiades Publishing, Ltd., 2022.

Crystal Field Parameters and Magnetic Properties Correlations in Rare-earth Orthoferrite $HoFeO_3$

O. V. Usmanov[a, *], A. K. Ovsianikov[a, b], I. A. Zobkalo[a], K. A. Shaykhutdinov[c, d], K. Yu. Terentjev[a, c], and S. V. Semenov[c, d]

[a] *Petersburg Nuclear Physics Institute by B.P. Konstantinov of NRC "Kurchatov Institute," Gatchina, 188300 Russia*

[b] *Institute of Crystallography, RWTH Aachen University, Aachen, 52066 Germany*

[c] *Kirensky Institute of Physics, Federal Research Center, Krasnoyarsk, 660036 Russia*

[d] *Siberian Federal University, Krasnoyarsk, 660071 Russia*

**e-mail: usmanov_ov@pnpi.nrcki.ru*

Received May 4, 2022; revised May 4, 2022; accepted May 4, 2022

Abstract—The crystal structure and magnetic properties investigations of holmium orthoferrite compound $HoFeO_3$ were performed in temperature range 7–300 K. Obtained XRD data confirm that $HoFeO_3$ retains the orthorhombic perovskite structure of *Pbnm* space group. The crystal electric field (CEF) parameters of Ho^{3+} ion subsystem has been revealed numerically on the base of point charge model in the same temperature range. By this set of parameters CEF the splitting of Ho^{3+} energy levels was calculated and their temperature evolution was obtained. Modelling of isothermal magnetization $M(H)$ with obtained set of parameters was carried out. Ho^{3+} single ion anisotropy due to CEF effects was demonstrated. Bulk magnetization evaluated from CEF was compared to experimental data.

Keywords: orthoferrites, X-ray powder diffraction, crystal electric field parameters, holmium orthoferrite, magnetization temperature evolution, CEF

DOI: 10.1134/S1027451022060258

1. INTRODUCTION

The unique magnetic properties of rare earth orthoferrites $RFeO_3$ (R – rare earth element) family arise as a result of complex interactions between the moments of 3*d* and 4*f* electrons. Studies of these magnetic compounds began several decades ago [1]. It was shown that crystal structure of all $RFeO_3$ compounds is described by the *Pbnm* space group [2], and magnetic structures of the members of this family were obtained by neutron powder diffraction [3]. According to these studies, $RFeO_3$ compounds have rather high Neel temperatures T_N ~ 600–700 K, below which the magnetic moments of Fe are ordered antiferromagnetically with a little tilt of the sublattices, that leads to weak ferromagnetism. As the temperature decreases, the role of the Fe–R interaction increases, and at lower temperatures—below the reorientation transition temperature T_{SR}, which lays most often in the range ~40–60 K—spin reorientation takes place. It should be mentioned that there are no such transitions for the non-magnetic ions R = Y, La, Lu [4]. Rare earth subsystem with a relatively weak R–R interactions is paramagnetic or weakly polarized by the molecular field of ordered Fe ions at high temperature. Magnetic sublattice of the rare earth becomes ordered below T_{NR} ~ 5–10 K. The complex magnetic properties of the total $RFeO_3$ system arise due to the multiplicity of different exchange interactions. In addition to the exchange interactions of the Heisenberg type like Fe–Fe, Fe–R, R–R, an important role in determining the magnetic properties is played by the Dzyaloshinsky-Moriya (DM) interaction [5, 6], which leads to the tilting of magnetic sublattices and causes the emergence of a weak ferromagnetic moment.

Last years the interest to this family has increased significantly due to the discovery of multiferroic properties in some compounds of this series. The appearance of ferroelectricity in them at temperatures below T_{NR} was predicted in the theoretical work [7] on the basis of a symmetry analysis of the crystal structure of these compounds. And indeed, in subsequent experiments in $DyFeO_3$ and $GdFeO_3$, the appearance of ferroelectric polarization below the ordering temperature of the rare-earth subsystem was observed [8, 9]. However, later ferroelectric polarization was observed in $DyFeO_3$ at relatively high temperatures—above T_{SR} [10], and in some orthoferrites—$SmFeO_3$ [11], $YFeO_3$

Table 1. Unit cell parameters (Å) within *Pbnm* space group

T, K	*a*	*b*	*c*
7	5.2680(1)	5.5825(1)	7.5845(1)
20	5.2710(1)	5.5859(2)	7.5909(2)
40	5.2674(4)	5.5821(4)	7.5847(6)
60	5.2719(1)	5.5865(1)	7.5919(2)
100	5.2715(2)	5.5867(2)	7.5925(3)
200	5.2746(1)	5.5884(1)	7.5961(2)
300	5.2778(1)	5.5908(1)	7.6016(2)

[12], $LuFeO_3$ [13] polarization was observed at room temperature, which brings these compounds closer to be used in high-tech devices. Macroscopic studies demonstrate a strong influence of external fields on the magnetic and/or ferroelectric properties of these compounds. Thus, in $DyFeO_3$, ferroelectric polarization is induced by the application of a magnetic field [8]. The application of an external electric field in compounds with R = $Dy_{0.70}Tb_{0.30}$, $Dy_{0.75}Gd_{0.25}$, according to magnetization measurements [14], led to the predominant orientation of domains with a certain direction of the weak ferromagnetic component and, thus, to the appearance of a macroscopic magnetic moment at $T < T_{NR}$. In $LuFeO_3$, the application of the external magnetic field led to decrease in the residual polarization in the ferroelectric hysteresis [13]. Also, a noticeable effect of an external magnetic field on the magnitude of electric polarization was observed in $TbFeO_3$ [15].

It should also be noted that the orthorhombic space group *Pbnm* (sometimes *Pnma* notation is used for this group) is centrosymmetric and does not allow spontaneous electrical polarization. In this regard, a more in-depth study of both the magnetic and crystalline properties of $RFeO_3$ compounds becomes a necessary element in the complex studies of the interactions of magnetic and ferroelectric order parameters.

Neel temperature in holmium orthoferrite $HoFeO_3$ is $T_N = 647$ K, below this temperature ordering of Fe sublattice takes place within the representation Γ_4, with configuration of magnetic moments $G_xA_yF_z$, where G_x is the strongest component and F_z is the weak ferromagnetic component. At $T_{SR} = 55$ K spin reorientation transition takes place to the Γ_1 phase with the configuration $A_xG_yC_z$. Weak ferromagnetism is forbidden in this phase. At lower temperature—$T_{SR2} = 35$ K one more spin reorientation takes place, the iron magnetic structure turns to Γ_2 phase. In this case configuration looks like $F_xA_yG_z$ [16], where *G*-component still is the strongest, that is *F* and *G* components changed places. The multiferroic features in $HoFeO_3$ were reported recently [17].

In the context of detailed studies of microscopic mechanisms that lead to multiferroicity in these materials, research of the crystal field effects along with magnetic investigations seems to be actual and relevant area of research that could give new deeper understanding about phenomena in $RFeO_3$ objects.

2. EXPERIMENTAL

High quality single crystals of $HoFeO_3$ have been grown by the optical floating zone technique (FZ-4000, Crystal Systems Corporation). They were used for magnetic studies. The orientation and quality of the crystals obtained was controlled using the Laue technique. For the samples for X-Ray measurements the crystals were taken from the same batch and then were crushed into powder. Powder X-Ray studies were performed at the Rigaku SmartLab diffractometer at the Petersburg Nuclear Physics Institute of NRC "Kurchatov Institute". Measurements of the magnetic properties were carried out at the Krasnoyarsk Regional Center of Research Equipment of Federal Research Center "Krasnoyarsk Science Center SB RAS" on the vibrating sample magnetometers Quantum Design PPMS—9T and Lakeshore VSM 8604.

3. RESULTS AND DISCUSSION

3.1. Crystal Structure Refinement

For the crystal structure refinement, the measurements at seven different temperatures were undertaken in order to elucidate whether there are differences in the crystal structure in different magnetically ordered phases. Then Rietveld refinement was made with the use of FullProf suite [18]. At all temperatures the diffraction patterns obtained witness that crystal structure is of orthorhombic distorted perovskite type with space group *Pbnm* (Table 1) without any noticeable hint of a secondary phase (Fig. 1). Unit cell parameters decrease smoothly with temperature decrease, as expected. In this unit cell both the Fe and Ho atoms occupy special positions 4b and 4c correspondingly.

The symmetry of the Fe position is $\bar{1}$ and ion Fe^{3+} coordinated by distorted oxygen octahedron. Ho ions are surrounded by eight nearest-neighbor distorted octahedra that provides local symmetry of Ho site 4c to be monoclinic C_s. The results of position refinement are shown at Table 2. It can be seen, that positions of Ho^{3+} ions change slightly with temperature decrease. At the same time the change of oxygen anions position is much more noticeable, that lead to

some noticeable changes in the surroundings of rare earth ion. Nevertheless, in all cases the symmetry of Ho site remains to be C_s.

3.2. Magnetization Studies

Figure 2a shows the temperature dependences of the magnetization $M(T)$ of $HoFeO_3$ measured at magnetic fields $H = 1$, 10, 30 kOe in the temperature range 4.2–100 K. The magnetic field was applied along the c axis of the crystal. Characteristic features on the $M(T)$ dependence measured at a field $H = 1$ kOe correspond to the spin-reorientation transition in $HoFeO_3$ which takes place at the temperature 55 K [28]. With an increase of the magnetic field H, the magnetic moments of iron sublattice are already polarized completely and the main contribution to the magnetization is made by the magnetic moments of holmium, while the magnetization monotonically increases with decreasing temperature.

On the Fig. 2b are shown the field dependences of the magnetization $M(H)$ measured at several temperatures in the range 4.2–100 K, i.e. above and below the spin-reorientation transition temperature. It can be seen the $M(H)$ dependences become linear as the temperature increases in the region of strong magnetic fields, and the feature in the region of weak magnetic fields is associated with the reorientation of the magnetic moments of iron. These results correlate well with those reported in [19], and quite similar behavior of magnetization was observed in $ErFeO_3$ [20].

3.3. CEF Hamiltonian, Calculations, Point-Charge Model

For evaluations of CEF parameters we consider effective Hamiltonian

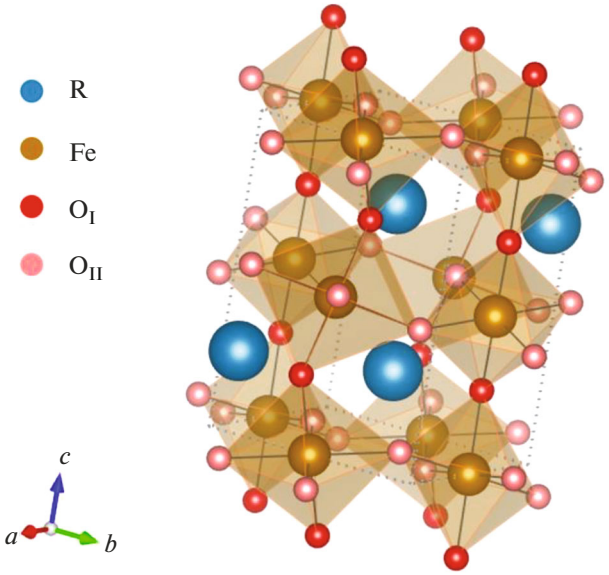

Fig. 1. $HoFeO_3$ unit cell.

$$H_{\mathrm{CEF}} = \sum_{l,m} B_l^m O_l^m, \qquad (1)$$

where B_l^m and O_l^m are Stevens coefficients and equivalent operators respectively [22]. As mentioned above, the Ho^{3+} ions occupy the low-symmetry position C_s. The point group C_s consists of two elements of symmetry—identity transformation E and the mirror plane σ_h. In the coordinate system with z axis perpendicular to σ_h, there no equivalent operators O_l^m with odd m in expansion (1) [24]. Hence, we consider the Hamiltonian with 15 independent B_l^m parameters:

Table 2. Positional parameters for different temperatures of measurements

T, K	Ho, 4c		O1, 4c		O2, 8d		
	x	y	x	y	x	y	z
7	0.9790(5)	0.0693(3)	0.0972(25)	0.4446(23)	0.6970(19)	0.3186(20)	0.0608(12)
20	0.9815(7)	0.0714(4)	0.0837(47)	0.4974(38)	0.7186(42)	0.3029(39)	0.0624(25)
40	0.9782(6)	0.0702(3)	0.0950(29)	0.4317(27)	0.7277(24)	0.3561(21)	0.0617(14)
60	0.9774(7)	0.0712(4)	0.1121(43)	0.4802(40)	0.7087(36)	0.3227(34)	0.0547(21)
100	0.9785(8)	0.0694(5)	0.1114(42)	0.4538(45)	0.6883(33)	0.2945(37)	0.0645(24)
200	0.9845(8)	0.0687(4)	0.1199(39)	0.4577(41)	0.6922(34)	0.2957(37)	0.0653(22)
300	0.9790(4)	0.0680(3)	0.0771(21)	0.4788(19)	0.6955(18)	0.3442(17)	0.0577(11)

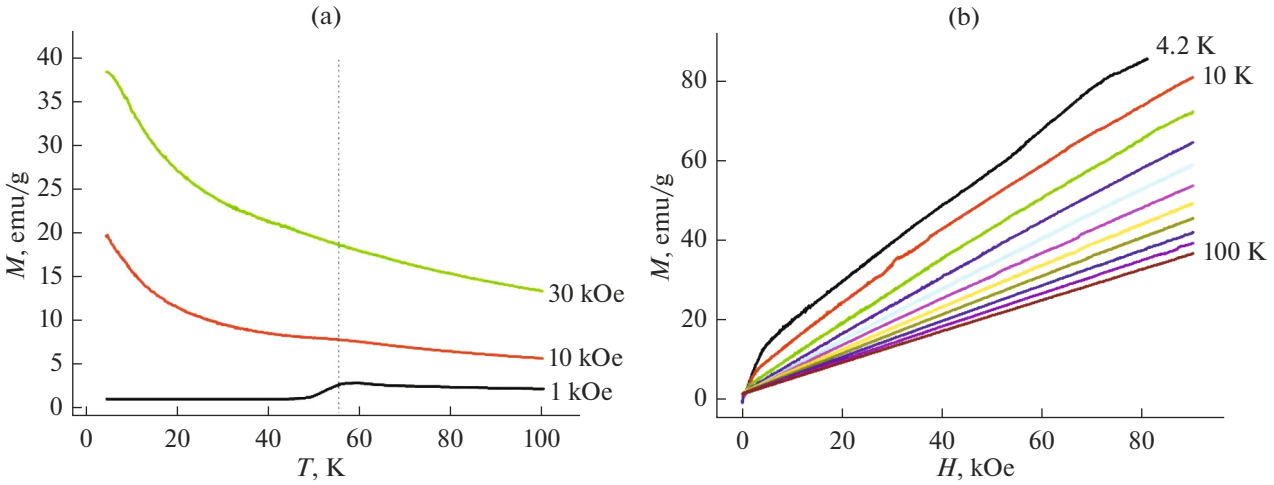

Fig. 2. Temperature dependence of the $HoFeO_3$ single crystal magnetization $M(T)$ for 3 different external magnetic fields (a). Field dependence of the $HoFeO_3$ single crystal magnetization $M(H)$ at different temperatures [28] (b).

$$H_{CEF} = B_2^0 O_2^0 + B_2^2 O_2^2 + B_2^{-2} O_2^{-2} + B_4^0 O_4^0 + B_4^2 O_4^2 + B_4^{-2} O_4^{-2} + B_4^4 O_4^4 + B_4^{-4} O_4^{-4} + B_6^0 O_6^0 + B_6^2 O_6^2 + B_6^{-2} O_6^{-2} + B_6^4 O_6^4 + B_6^{-4} O_6^{-4} + B_6^6 O_6^6 + B_6^{-6} O_6^{-6}. \quad (2)$$

For the quantitative evaluation of CEF Hamiltonian here we use a point-charge model (PC) [21–23]. This is a pretty rough model [26, 27] which takes into account only Coulomb interaction and neglects possible screening or orbital hybridization. But for the ionic crystals containing elements with localized 4*f* elec-

Table 3. Set of B_l^m parameters calculated from the PC model

B_l^m, meV		T, K				
		7	40	60	100	300
B_2^0	$\times 10^{-1}$	0.93	1.36	1.18	0.77	−0.23
B_2^2		3.69	2.55	3.28	2.70	1.35
B_2^{-2}		−2.74	−3.99	−3.89	−3.59	−3.44
B_4^0	$\times 10^{-3}$	0.05	0.05	0.06	0.05	0.08
B_4^2		0.03	−0.37	−0.18	−0.08	0.26
B_4^{-2}		−0.83	−1.02	−1.13	−1.16	−1.45
B_4^4		0.40	0.63	0.50	0.52	0.12
B_4^{-4}		1.92	1.61	1.65	1.76	1.24
B_6^0	$\times 10^{-5}$	0.10	0.10	0.10	0.10	0.10
B_6^2		−0.10	−0.10	−0.10	−0.20	−0.30
B_6^{-2}		−0.40	−0.30	−0.30	−0.30	−0.40
B_6^4		2.00	2.20	2.30	2.20	2.10
B_6^{-4}		0.00	−0.80	−0.30	−0.30	0.30
B_6^6		−0.20	−0.20	−0.10	−0.20	−0.30
B_6^{-6}		−0.60	−0.40	−0.40	−0.30	−0.10

Table 4. The energy levels of Ho^{3+} obtained from PC model

E, meV	T, K				
	7	40	60	100	300
$\|E_0\rangle \to \|E_1\rangle$	0.00	0.00	0.00	0.01	0.16
$\|E_0\rangle \to \|E_2\rangle$	18.34	18.71	17.86	14.77	3.99
$\|E_0\rangle \to \|E_3\rangle$	18.37	18.71	17.88	14.82	4.35
$\|E_0\rangle \to \|E_4\rangle$	30.16	31.26	31.13	26.56	15.26
$\|E_0\rangle \to \|E_5\rangle$	30.34	31.34	31.27	26.77	15.97
$\|E_0\rangle \to \|E_6\rangle$	39.65	42.50	43.09	37.62	23.62
$\|E_0\rangle \to \|E_7\rangle$	40.01	43.06	43.62	38.11	25.00
$\|E_0\rangle \to \|E_8\rangle$	45.44	50.03	51.03	44.55	29.26
$\|E_0\rangle \to \|E_9\rangle$	46.24	50.76	51.78	45.57	31.45
$\|E_0\rangle \to \|E_{10}\rangle$	49.27	54.14	55.61	49.17	33.45
$\|E_0\rangle \to \|E_{11}\rangle$	51.08	55.78	57.10	49.25	36.34
$\|E_0\rangle \to \|E_{12}\rangle$	52.89	57.02	58.85	51.08	36.82
$\|E_0\rangle \to \|E_{13}\rangle$	57.82	60.28	62.49	54.23	39.29
$\|E_0\rangle \to \|E_{14}\rangle$	58.86	60.73	63.41	55.14	39.34
$\|E_0\rangle \to \|E_{15}\rangle$	59.49	64.87	65.15	55.74	45.96
$\|E_0\rangle \to \|E_{16}\rangle$	60.04	64.99	65.53	56.29	45.98

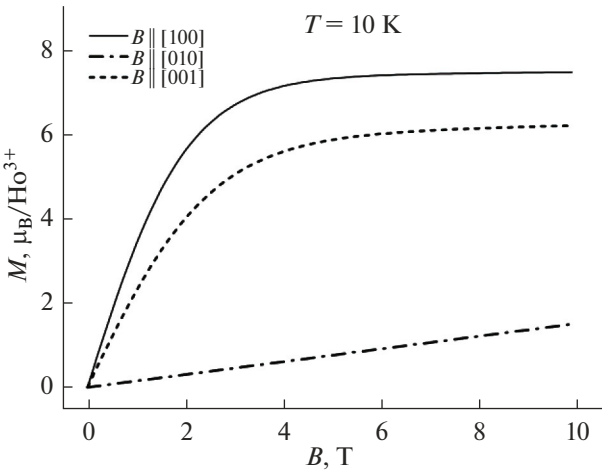

Fig. 3. Calculated magnetization of Ho^{3+} ions according to the crystal structure data at $T = 10$ K.

trons it can provide a satisfactory estimation of the CEF parameters.

For CEF calculations with the use of PC model we utilized McPhase [23] and PyCrystalField [25] software packages. In course of treatment we considered neighboring ions within a sphere of radius 5.98 Å, and obtained set of parameters presented at Table 3. Here one could pay attention on the B_2^m ($m = -2, 0, 2$) parameters since they are responsible for the principal terms of Hamiltonian (2) and in a great degree determine the splitting energy of ground state multiplet. They show strong anisotropy of Ho magnetization that is caused by interaction of rare-earth subsystem and CEF, especially at low temperatures. One can pay attention also to the significant difference in the value of B_2^2 at 60 K, i.e. in the vicinity of SR transition and at other temperatures.

Crystal field parameters B_l^m are responsible for the splitting of the ground multiplet in the crystal field and they are very sensitive to tiny displacements of the surrounding atoms and certainly, to the change of local symmetry. It is known, that single-ion anisotropy is associated with the fact that the energy of a magnetic ion, due to the splitting of orbital levels by the crystal field, depends on the orientation of the orbital momentum with respect to crystallographic axes, and, consequently, due to the spin-orbit interaction, depends on the orientation of the spin relative to these axes. By the use of the set from Table 3, we obtained CEF splitting of the ground $^5I_8$ multiplet of the $4f^{10}$ configuration of non-Kramers ion Ho^{3+}. Our calculations clearly show that the CEF fully lifts the degeneracy of the ground state multiplet into quasi-doublet structure of the energy levels (Table 4).

CEF calculations of magnetization of Ho^{3+} subsystem showed that it is strongly anisotropic with easy plain *ac* (Fig. 3), the calculated dependence qualitatively repeats the experimentally measured one in work [28].

In order to check the reliability of the obtained parameters, the calculations of the bulk magnetization along [001] direction were performed and then comparison of the calculated and measured dependencies was made. The experimental and calculated magnetization dependencies for 40 and 60 K are shown at the Fig. 4 as example.

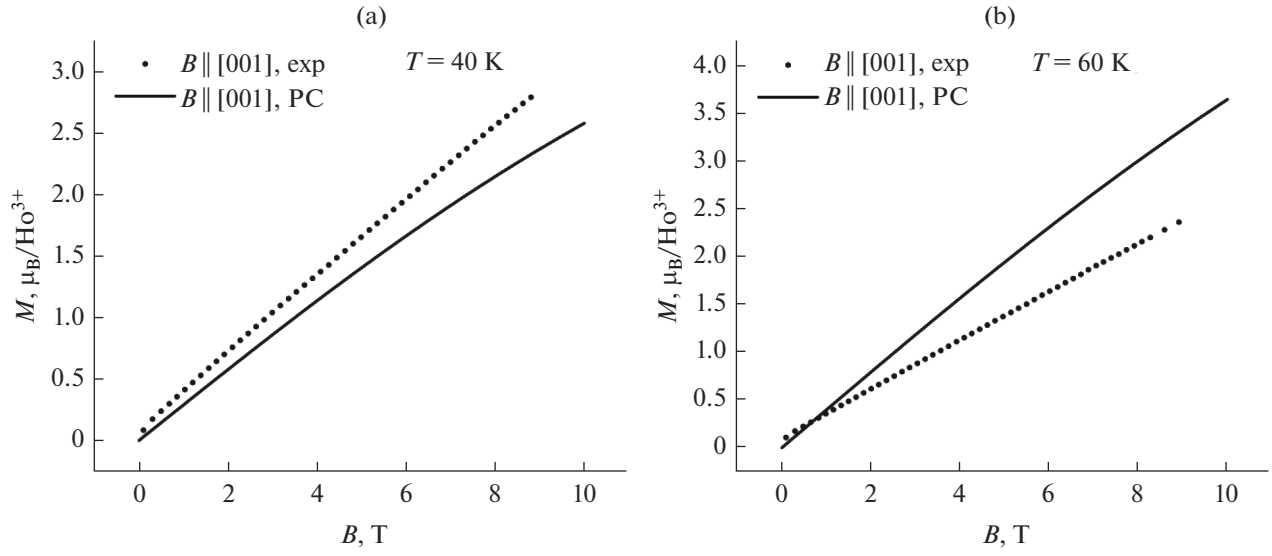

Fig. 4. Comparison of calculated and measured magnetization along the *c* axis of crystal (at $T = 40$, 60 K).

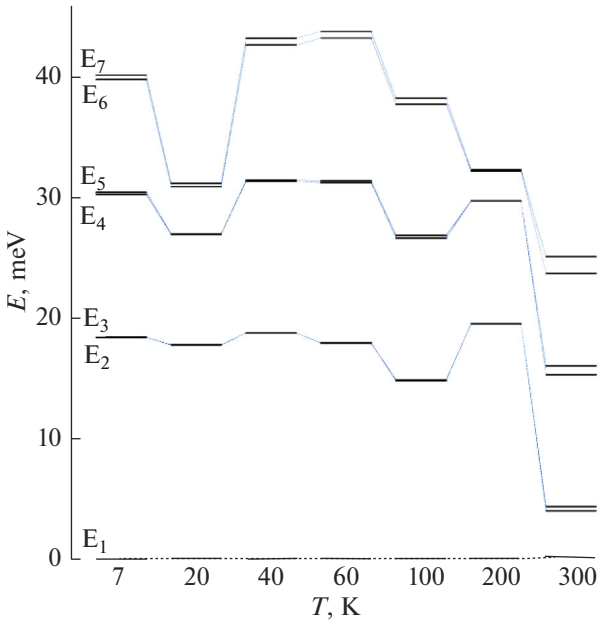

Fig. 5. Temperature evolution of first seven energy levels obtained from PC model (see Table 4). There can be seen the quasidoublet series after the first excited energy level E_1.

Ho^{3+} ions magnetization obtained on the base of PC model, reproduces well the measured experimental points, though definite disagreement can be seen. This could be caused by a contribution of the Fe magnetic sublattice, and due to Fe–Ho interactions which were not considered in simple PC model.

The Fig. 5 illustrates temperature dependence of first excited energy levels obtained from PC calculations, which can reflect the significant changes in Ho^{3+} ion surrounding, especially near the SR temperature at 55 K (see Table 2, positions of surrounding oxygen ions).

ACKNOWLEDGMENTS

Authors express their gratitude to A. Bykov for the help with XRD measurements and S. Skorobogatov for advisory assistance.

FUNDING

This work was supported by the Russian Foundation for Basic Research grant no. 19-52-12047, and DFG grant no. SA 3688/1-1.

CONFLICT OF INTEREST

The authors declare that they have no conflict of interest.

REFERENCES

1. R. White, J. Appl. Phys. **40**, 1061. (1969). https://doi.org/10.1063/1.1657530
2. M. Marezio, J. P. Remeika, and P. D. Dernier, Cryst. Acta B **26**, 2008 (1970). https://doi.org/10.1107/S0567740870005319
3. W. C. Koehler, E. O. Wollan, and M. K. Wilkinson, Phys. Rev. **118**, 58 (1960). https://doi.org/10.1103/PhysRev.118.58
4. K. Park, H. Sim, J. C. Leiner, Y. Yoshida, J. Jeong, S. Yano, J. Gardner, P. Bourges, M. Klicpera, V. Sechovský, M. Boehm, and J. Park, J. Phys.: Condens. Matter. **30**, 235802 (2018). https://doi.org/10.1088/1361-648X/aac06b
5. I. E. Dzyaloshinsky, J. Phys. Chem. Solids. **4**, 241 (1958). https://doi.org/10.1016/0022-3697(58)90076-3
6. T. Moriya, Phys. Rev. **120**, 91 (1960). https://doi.org/10.1103/PhysRev.120.91
7. A. K. Zvezdin and A. A. Mukhin, JETP Lett. **88**, 505 (2008). https://doi.org/10.1134/S0021364008200083
8. Y. Tokunaga, S. Iguchi, T. Arima, and Y. Tokura, Phys. Rev. Lett. **101**, 097205 (2008). https://doi.org/10.1103/PhysRevLett.101.097205
9. Y. Tokunaga, N. Furukawa, H. Sakai, Y. Taguchi, T. Arima, and Y. Tokura, Nat. Mater. **8**, 558 (2009). https://doi.org/10.1038/nmat2469
10. B. Rajeswaran, D. Sanyal, M. Chakrabarti, Y. Sundarayya, A. Sundaresan, and C. N. R. Rao, Europhys. Lett. **101**, 17001 (2013). https://doi.org/10.1209/0295-5075/101/17001
11. J.-H. Lee, Y. K. Jeong, J. H. Park, M.-A. Oak, H. M. Jang, J. Y. Son, and J. F. Scott, Phys. Rev. Lett. **107**, 117201 (2011). https://doi.org/10.1103/PhysRevLett.107.117201
12. C. Kuo-Y., Y. Drees, Fernández-M. T. Díaz, L. Zhao, L. Vasylechko, D. Sheptyakov, A. M. BellT., T. W. Pi, H. Lin-J., M. Wu-K., E. Pellegrin, S. M. Valvidares, Z. W. Li, P. Adler, A. Todorova, R. Küchler, A. Steppke, L. H. Tjeng, Z. Hu, and A. C. Komarek, Phys. Rev. Lett. **113**, 217203 (2014). https://doi.org/10.1103/PhysRevLett.113.217203
13. U. Chowdhury, S. Goswami, D. Bhattacharya, J. Ghosh, S. Basu, and S. Neogi, Appl. Phys. Lett. **105**, 052911 (2014). https://doi.org/10.1063/1.4892664
14. Y. Tokunaga, Y. Taguchi, T. Arima, and Y. Tokura., Nat. Phys. **8**, 838 (2012). https://doi.org/10.1038/nphys2405
15. Y.-Q. Song, W.-P. Zhou, Y. Fang, Y.-T. Yang, L.-Y. Wang, D.-H. Wang, and Y.-W. Du, Chin. Phys. B **23**, 077505 (2014). https://doi.org/10.1088/1674-1056/23/7/077505
16. T. Chatterji, M. Meven, and P. J. Brown, AIP Adv. **7**, 045106 (2017). https://doi.org/10.1063/1.4979710
17. K. Dey, A. Indra, S. Mukherjee, S. Majumdar, J. Strempfer, O. Fabelo, E. Mossou, T. Chatterji, and S. Giri, Phys. Rev. B **100**, 214432 (2019). https://doi.org/10.1103/PhysRevB.100.214432

18. J. Rodriguez-Carvajal, Phys. B (Amsterdam, Neth.) **192**, 55 (1993). https://doi.org/10.1016/0921-4526(93)90108-I

19. M. Shao, S. Cao, Y. Wang, S. Yuan, B. Kang, and J. Zhang, Solid State Commun**152**, 947 (2012). https://doi.org/10.1016/j.ssc.2012.03.030

20. R. Huang, S. Cao, W. Ren, S. Zhan, B. Kang, and J. Zhang, Appl. Phys. Lett. **103**, 162412 (2013). https://doi.org/10.1063/1.4825274

21. K. W. H. Stevens, Proc. Phys. Soc., London, Sect. A **65**, 209 (1952). https://doi.org/10.1088/0370-1298/65/3/308

22. M. T. Hutchings, in *Solid State Physics: Advances in Research and Applications*, **Vol. 16**, Ed. by F. Seitz and D. Turnbull (Academic, New York, 1964).

23. M. Rotter, J. Magn. Magn. Mater. **272–276**, E481 (2004). https://doi.org/10.1016/j.jmmm.2003.12.1394

24. A. K. Zvezdin, V. M. Matveev, A. A. Mukhin, and A. I. Popov, *Rare Earth Ions in Magnetically Ordered Crystals* (Nauka, Moscow, 1985) [in Russian].

25. A. Scheie, J. Appl. Cryst. **54**, 356 (2021). https://doi.org/10.1107/S160057672001554X

26. S. Edvardsson and M. Klintenberg, J. Compd. Alloys **275–277**, 230 (1998). https://doi.org/10.1016/S0925-8388(98)00309-0

27. J. Mesot and A. Furrer, in N*eutron Scattering in Layered Copper-Oxide Superconductors: Physics and Chemistry of Materials with Low-Dimensional Structures*, Vol. 20, Ed. by A. Furrer (Springer, Dordrecht, 1998). https://doi.org/10.1007/978-94-015-1284-8_9

28. A. Ovsianikov, O. Usmanov, I. Zobkalo, V. Hutanu, S. Barilo, N. Liubachko, K. Shaykhutdinov, K. Terentjev, S. Semenov, T. Chatterji, M. Meven, P. J. Brown, G. Roth, L. Peters, H. Deng, and A. Wu, J. Magn. Magn. Mater. **557**, 169431 (2022). https://doi.org/10.1016/j.jmmm.2022.169431